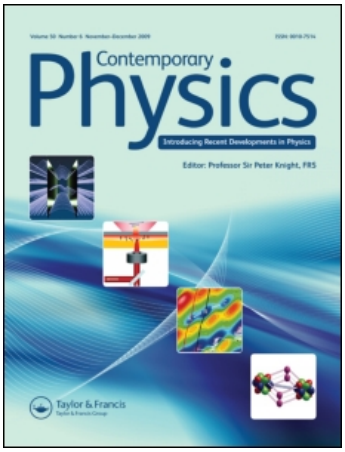

Contemporary Physics
Publication details, including instructions for authors and subscription information:
http://www.informaworld.com/smpp/title~content=t713394025

Photons and (artificial) atoms: an overview of optical spectroscopy techniques on quantum dots

A. N. Vamivakas [a]; M. Atatüre [a]
[a] Cavendish Laboratory, University of Cambridge, Cambridge, UK

Online publication date: 15 December 2009

To cite this Article Vamivakas, A. N. and Atatüre, M.(2010) 'Photons and (artificial) atoms: an overview of optical spectroscopy techniques on quantum dots', Contemporary Physics, 51: 1, 17 — 36
To link to this Article: DOI: 10.1080/00107510903298198
URL: http://dx.doi.org/10.1080/00107510903298198

Contemporary Physics
Vol. 51, No. 1, January–February 2010, 17–36

Taylor & Francis
Taylor & Francis Group

Photons and (artificial) atoms: an overview of optical spectroscopy techniques on quantum dots

A.N. Vamivakas and M. Atatüre*

Cavendish Laboratory, University of Cambridge, JJ Thomson Avenue, Cambridge CB3 0HE, UK

(*Received 27 March 2009; final version received 6 August 2009*)

In most branches within experimental physics technical prowess lies at the heart of many seminal works. From the observation of the photoelectric effect and the ultraviolet catastrophe that led to the development of quantum mechanics to the first transistor that shaped the modern age of electronics, significant physical insight has been achieved on the shoulders of technical advances and progress. Research on self-assembled quantum dots may be a drop in the sea of physics, but it still is no exception to this trend, and more physical insight continues to be revealed as the tools of the trade get increasingly more complex and advanced. This article is written primarily for senior undergraduate students and first year graduate students of experimental physics involving optically active quantum dots. More often than not, we have seen students shuffling through journal articles trying to relate the reported physics to the used experimental techniques. What we want to cover here is not in any way the history or the recent progress in quantum dot research – there are an ample number of topical books and review articles for that – but rather to highlight a selection of optics-based measurement techniques that have led to significant progress in our understanding of quantum dot physics as well as their applications in the last two decades. We hope a basic survey of the relevant optical spectroscopy techniques will help the newcomers in connecting the *dots* between measurements and physics.

Keywords: quantum dots; excitons; spectroscopy; quantum optics; quantum information science

1. Introduction

Quantum dots have become a system of study in a broad range of disciplines in a relatively short time. The incredible progress in synthesis, growth and fabrication quality fed further the advances in optical investigations in physics, biology and chemistry. Particular to quantum physics, quantum dots allow optical studies of confined charge and spin systems and in parallel studies on engineering light–matter interaction and even the suppression of spontaneous emission. We start below with an introduction to the growth of quantum dots and then follow with a discussion of the various optically active charge complexes that a quantum dot can support. We then proceed with a handful of optical techniques lined up vaguely with increasing technical difficulty and chronological appearance. We finish with a selection of applications, mainly driven by quantum information science, in order to highlight how much experimental progress in quantum information science is indeed driven by a reinterpretation of results obtained via conventional optical spectroscopy.

2. Quantum dots: from growth to energy levels

Advances in material science have enabled the growth of heterostructures exhibiting inhomogeneity on a length scale relevant for influencing the spectrum of a material's excitations. Quantum dots (QDs) are heterostructures engineered to provide three-dimensional spatial confinement for electronic excitations. The confinement yields a discrete spectrum of QD energy eigenstates and it is not uncommon to refer to QDs as *artificial atoms*. In practice, there exist a number of quantum confined physical systems that exhibit a discrete electronic spectrum – interface fluctuation QDs that form at the gallium arsenide/aluminum gallium arsenide (GaAs/AlGaAs) barrier boundary in a quantum well, core–shell cadmium selenide/zinc sulphide (CdSe/ZnS) nanocrystals formed through both colloidal methods and quantum dots grown by Metallic Organic Vapour Phase Epitaxy (MOVPE), electrically defined QDs via gate electrodes patterned on two-dimensional electron gas yielding precise control over the local electrostatic potential and self-assembled QDs grown by Molecular Beam Epitaxy (MBE). Here, we will focus mainly, but not exclusively, on indium arsenide (InAs)/GaAs self-assembled QDs in portraying the optical techniques used to date. In this section, before looking into the characteristic electronic structure of QDs, we will discuss the material science advances that have resulted in the growth of self-assembled QDs by MBE.

*Corresponding author. Email: ma424@cam.ac.uk

ISSN 0010-7514 print/ISSN 1366-5812 online

DOI: 10.1080/00107510903298198
http://www.informaworld.com

Epitaxial growth is a process where a new crystal is grown over a host crystal surface via layer-by-layer atomic deposition [1]. Epitaxial techniques are capable of depositing high quality semiconductors with an abrupt change in material composition having monolayer ($\sim$3 Å) accuracy. The formation of InAs/GaAs QDs is a natural process and is the manifestation of a strain-driven phase transition that occurs when combining two materials of different lattice constants during one material growth cycle. Every material has its own lattice constant and this commonly leads to formation of strain on two layers constituting an abrupt interface. Figure 1(*a*) illustrates the two typical cases of strain release: a monolayer-thick material embraces a lattice constant dictated by the host material or a sufficiently thick material recovers its own lattice constant resulting in strain release via dislocations and defects at the interface. The formation occurs exactly during the transitional period linking the two regimes of strain release. If the lattice constants are significantly different (e.g. 7% mismatch between l_a and l_b, as is the case for GaAs and InAs lattices), the epitaxial growth of InAs with the GaAs lattice can not be sustained for more than two monolayers of growth. At one point, the newly formed layer goes through a phase transition forming miniature islands, very much like mercury droplets do on a smooth flat surface. Further growth with the same material as the handle wafer, in this case GaAs, caps the QDs and protects them from the surrounding environment. After growth, the height of the QDs is typically 4–5 nm, as determined by cross-sectional scanning tunnelling microscopy image of Figure 1(*b*) [2]. We emphasise that, although the self-assembled QDs exhibit pristine optical properties, the in-plane QD distribution is disordered and extensive efforts are still made today in this field in order to achieve better control over the island size distribution and location of nucleation.

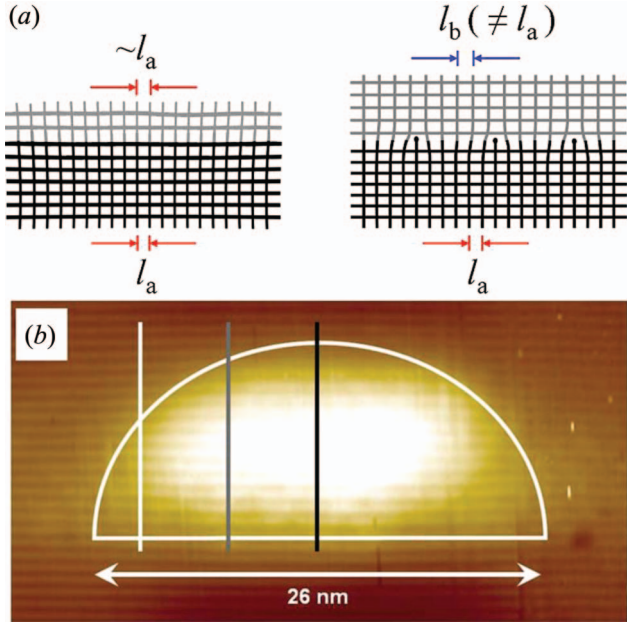

Figure 1. (*a*) An illustration of lattice constant mismatch for two materials grown by MBE for strained thin layers and dislocated thick layers. (*b*) Cross-sectional scanning tunnelling microscopy of a self-assembled InAs QD grown by MBE [2].

The MBE growth process results in strong three-dimensional carrier confinement for electrons in QDs resulting in quantisation of energy states. However, QDs are composed of around 10^5 atoms, and thus form a mesoscopic system with arbitrary shape and composition which differ from QD to QD. The distribution in shape and composition combined with the strain profile experienced by the QD all influence the single particle QD energy levels in the form of inhomogeneous broadening. In addition to material properties, if multiple charges are confined in the QD the Coulomb interaction between the quantum confined carriers has to be taken into account when calculating the multi-particle energy levels. All the previous complications make an analytical determination of QD properties practically impossible and modelling typically relies on perturbative or numerical methods. Even with all these complications it is striking that the roughly 10^5 InAs atoms in the GaAs matrix conspire to exhibit a discrete atomic-like energy spectrum.

The InAs/GaAs QDs covered in this work are semiconductors in bulk (three-dimensional) form. Therefore, to solve for the energy levels of QDs, it is natural to start from the bulk material properties and determine the consequences of reducing the system's dimensionality. For a phenomenological, but satisfactory, prediction of bulk semiconductor band structures, we resort to a perturbative $\boldsymbol{k} \cdot \boldsymbol{p}$ model. In $\boldsymbol{k} \cdot \boldsymbol{p}$ single-particle wavefunctions and energy eigenvalues are assumed to be known at $\boldsymbol{k} = 0$ and the band dispersion is obtained in the small $\boldsymbol{k}$ approximation around the Γ -point [3]. These perturbative methods can also be applied to quantum dots since the $\boldsymbol{k}$-vector distribution of confined charges is concentrated around $\boldsymbol{k} = 0$. Figure 2 shows a schematic of the band structure of bulk GaAs with relevant parameter values at room temperature. The band structure of InAs looks esentially identical, but, the values of the indicated parameters differ significantly from GaAs.

Excitation of an electron across the bandgap leaves an empty electronic state in the otherwise electron-filled valence band. These *holes* can equally be treated as positively charged particles with modified mass and g-factor. The lowest conduction band has to a very good approximation parabolic dispersion around the

Γ -point, as indicated by the red curve in Figure 2. The wavefunctions for this band have s-wave character sustaining a twofold spin-degeneracy with $[S||S_z] = [1/2|| \pm 1/2]$. The valence band wavefunctions have p-wave character that would normally sustain a sixfold spin-degeneracy forming a $[3/2|| \pm 3/2, \pm 1/2]$ quadruplet and $[1/2|| \pm 1/2]$ doublet. However, spin-orbit coupling in these semiconductors causes the $[1/2|| \pm 1/2]$ doublet to be separated in energy forming what is referred to as the split-off band (Figure 2). Further, upon including the influence of other bands, even the fourfold degeneracy of the $[3/2|| \pm 3/2, \pm 1/2]$ states is lifted for $\boldsymbol{k} \neq 0$ forming the heavy-hole and the light-hole bands with near-parabolic *negative* curvature dispersion as seen in Figure 2.

When the dimensionality of the system is reduced such that the effective Bohr radius becomes comparable to the physical extent of the confining material, quantum confinement strongly influences the density of states, band dispersion and degeneracies. In the case of QDs, the dimensionality is zero resulting in motional confinement along all three directions. Therefore, a set of discrete energy levels arise with level spacings determined by the, not necessarily equal, confinement strength along each direction. In fact, due to their particular lens-like topology (see Figure 1(*b*)), the QDs considered here display strongest motional confinement along the growth (z) axis. Therefore, the main features of the energy levels of these QDs can be seen by simply considering a strong confinement along the z direction with a two-dimensional quasi-parabolic confinement in the two remaining directions. A generally accepted approach to quantifying the QD energy levels and the corresponding wavefunctions relies on pseudopotential theory [4]. A nice tutorial discussion of pseudopotential theory, with illustrations of the QD electronic excitation wavefunctions, can be found in the review by Zunger [5].

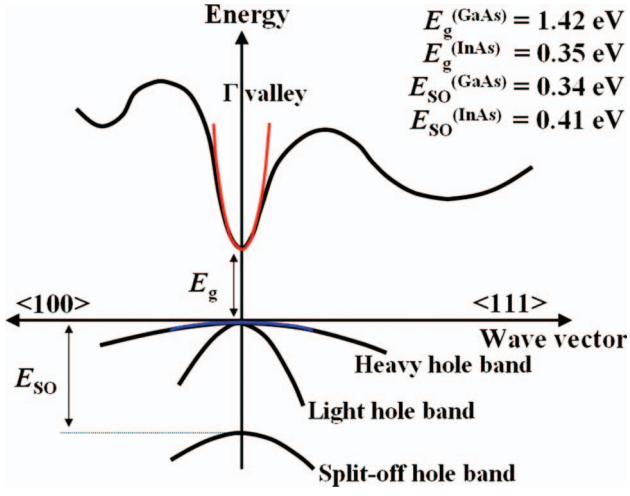

Figure 2. A simplified band structure illustration for III–V semiconductors such as GaAs and InAs with the typically accepted values for key energy scales.

From the optics perspective an important feature of the quantum confinement is that although the energy spectrum of the QD is altered when compared to the bulk semiconductor, the electrons and holes that become trapped in the QD inherit the spin structure of the bulk semiconductor. This determines the optical (polarisation) selection rules for transitions between QD electron and hole states mediated by a photon. Explicitly, focusing on the conduction band and heavy hole valence band, we can specify the QD electron and hole spin. The QD levels derived from the conduction band levels sustain their twofold spin degeneracy, while the QD levels derived from the valence band states display a confinement-induced splitting into heavy-hole and light-hole doublets.

We qualitatively established the energy levels of electrons and holes confined in all three dimensions in semiconductor QDs. We now identify the energy scales of common InAs/GaAs QD charge configurations that are probed optically. The simplest charge configuration linked to an optical emission is the *neutral* exciton X^0 (see Figure 3), i.e. a single electron–hole pair occupying the lowest discretised energy levels

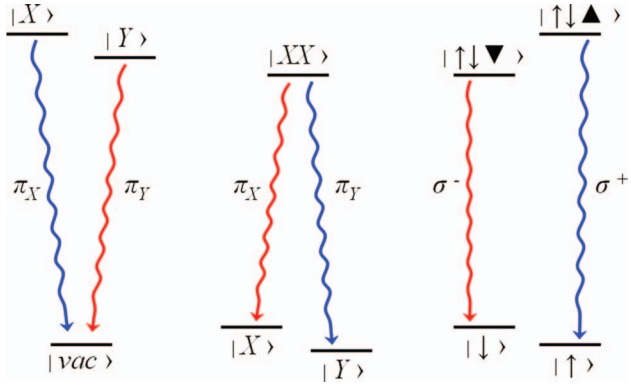

Figure 3. Neutral exciton (X^0), biexciton (XX) transitions under excitonic level splitting and negatively charged trion (X^{1-}) transitions under magnetic field along the growth axis for a typical quantum dot. The wavy arrows indicate photon mediated transitions between the states. For the negatively charged trion (right illustration) the up (down) arrow represents the electron spin projection of $+1/2$ ($-1/2$) along the growth direction and the solid up (down) triangle is the hole projection of $+3/2$ ($-3/2$). The ground state of the trion transition is a single electron with its spin projection up or down. Each transition is decorated with a symbol indicating the emitted photons polarisation – π_X (π_Y) for horizontal (vertical) and σ^+ (σ^-) for right (left) circularly polarised photons. The direction of linear polarisation (horizontal and vertical) is defined with respect to the major and minor axis of the elliptical QD base (as opposed to circular) due to strain-induced anisotropy of the dot geometry.

within the original conduction and valence bands. The electron in the conduction band can have spin quantum number $[S||S_z] = [1/2|| \pm 1/2]$. The heavy hole in the valence band has spin $[J||J_z] = [3/2|| \pm 3/2]$. By addition of angular momentum, a single electron–hole pair in the QD can end up in any one of four spin-state combinations. The total angular momentum of these combinations being $\Delta J = \pm 1$ or $\Delta J = \pm 2$, each doublet is degenerate. In an optical transition angular momentum must be conserved, and this is reflected in the polarisation of the emitted photons. Recombination via a single-photon emission process can only occur for the $\Delta J = \pm 1$ exciton doublet, since single photons carry angular momentum ± 1. The angular momentum conservation is reflected in the emitted photon's polarisation. Specifically, photons carrying $+1$ (-1) angular momentum are left (right) hand circularly polarised and are denoted with the symbol σ^+ (σ^-). The exciton doublet $\Delta J = \pm 1$ that is linked to photon emission is called *bright*, while the remaining optically inactive doublet is called *dark* (the $\Delta J = \pm 2$ excitons). The polarisation selection rules also constrain the set of excitons that may be created optically to the $\Delta J = \pm 1$ doublet.

Of course, the real world is not simple! The previously mentioned shape nonuniformity and strain act to coherently mix the bright $\Delta J = \pm 1$ exciton doublet via the electron–hole exchange interaction. This interaction couples the spins of the electron and hole confined in the QD and depends sensitively on the structural symmetry of the QD. The electron–hole exchange serves to both break the $\Delta J = \pm 1$ exciton doublet's degeneracy and alter the polarisation of the emitted photons from circular to linear, indicated by π_X/π_Y in Figure 3. This new polarisation basis, which is defined along the major and minor axis of the elliptical QD base, led to the phrase $X - Y$ splitting to denote this effect. Due to exchange interaction, an electron–hole pair once created in $\Delta J = +1$ state will precess coherently between $\Delta J = \pm 1$ spin configurations. A re-diagonalised Hamiltonian after including this interaction leads to new eigenstates with the degeneracy of their energies lifted in proportion to the interaction strength. Typical energy scale for the $\Delta J = \pm 1$ exciton doublet fine structure splitting is ~ 10 μeV for self-assembled InAs/GaAs QDs. We will see this fine-structure splitting has consequences for applications involving photon emission in later sections of this article. We direct the reader to [6] for a complete discussion of electron–hole exchange interaction.

The next QD charge complex we discuss is two electrons and one hole. We call this singly *charged* excitonic QD excited state a *trion*, see Figure 3 (right diagram), and label it as X^{1-}. In forming the trion complex, Pauli's principle forces the electron pair to form a spin singlet state where the closest triplet state has energy much higher than typical ambient temperature (4 K). Since the resident hole can have either spin up or spin down, each QD has two trionic transitions that are energetically degenerate. Due to Coulomb interactions in this three-body problem, the recombination energy is modified with respect to the original neutral X^0 excitonic transition energy (ignoring fine structure) by $\Delta E = E_{ee} - E_{\mathrm{eh}}$ – the direct energy due to electron–electron and electron–hole Coulomb interaction [7] as dictated by the wavefunctions via the form

$$E_{mn} \propto \frac{(-1)^{(1-\delta_{m,n})} e^2}{4\pi\varepsilon_0\varepsilon_r} \iint dr dr' \frac{|\psi_m(r)|^2 |\psi_n(r')|^2}{|r - r'|}. \quad (1)$$

In the InAs/GaAs QDs considered here the result is a total shift of $\Delta E = 6$ meV to lower energy for the trionic transitions. In contrast to the neutral exciton where the electron–hole spin exchange breaks the twofold degeneracy, the electronic spin singlet is immune to electron–hole exchange and the two trion states remain degenerate. In this case, the polarisation of the emitted photon is in the circular basis and the handedness is determined the direction of the resident hole spin.

The situation is conceptually similar when there are two electron–hole pairs present in the QD referred to as the *biexciton* (XX) shown in Figure 3 (middle diagram). The shift in the transition energy for a biexcitonic transition can once more be determined by the energy difference between the initial and final states, $\Delta E = 2E_{\mathrm{ee}} + 2E_{\mathrm{hh}} - E_{\mathrm{eh}}$, and is on the order of 2 meV for InAs QDs. Ultimately, every charge combination results in a distinct spectral signature due to the Coulomb interaction, and we refer the reader to [7] for a detailed explanation of this approach for direct and exchange type interactions.

It is good to note here that the relevant energy scales for each mechanism considered are well defined. The optical transitions occur at eV range while direct Coulomb interactions within a QD are at tens of meV. The fine structure such as X–Y splitting as we will see later is on the order of tens of μeV, which is still much larger than the characteristic transition linewidth of 1 μeV. While each quantum dot can have vastly different emission energies due to inhomogeneity in the quantum dot ensemble, the relative energy shifts are conveniently rather robust. With an understanding of common QD charge complexes, we can begin to address how the tools of optical spectroscopy reveal physical properties of the QD states.

3. Optical spectroscopy techniques

In the previous section we highlighted the most relevant excitonic complexes in QD optics and their

relevant energy scales. How excitons and photons couple to each other can be presented in many ways. We will make a distinction between two methods of optical excitation. The first approach, which we refer to as nonresonant excitation, is to use a light source, typically a laser, with an energy that is larger than the energy of the relevant excitonic transition. The laser creates exciton population in either higher energy QD excitons or in the bulk of the host semiconductor matrix. The higher energy excitons then nonradiatively relax, giving off energy through carrier scattering and phonons, and populate the lowest energy available exciton state. The second approach is to use a laser with energy equal to the excitonic state of interest much like in atomic physics. In the latter case we will say the laser is resonant to conform to the language used in the field. Of course either method of excitation links real states of the system and is resonant; but we rather use the term resonant to indicate a laser that has energy commensurate with the relevant exciton transition.

3.1. *Optics of quantum dots: nonresonant excitation*

3.1.1. *Exciton spectrum – photoluminescence*

A quantum dot may host discretised electronic levels, but the surrounding semiconductor matrix introduces a continuum of filled valence and available conduction band states. Therefore, an optical field can generate an ensemble of electron–hole pairs in the vicinity of a quantum dot. Typically, most of these pairs recombine quickly to yield photon generation at the bandgap energy of the semiconductor, while occasionally, a combination of electrons and holes may be captured into the discrete exciton levels of the quantum dot. For this to happen, the excess energy of the excitons has to be taken away by carrier scattering or phonons. Exactly how this relaxation occurs and how it depends on external parameters such as temperature and magnetic field has formed a whole branch of research on quantum dots, especially in the 1990s. This relaxation process happens at relatively fast timescales, i.e. tens of picoseconds and removes any coherence with the excitation laser. Therefore, generation of excitons in a quantum dot via bandgap excitation can be treated typically by an incoherent driving field between quantum dot states. In addition, the spin orientations of the optically excited electrons and holes are affected during the relaxation processes yielding only a residual correlation to the original excitation laser polarisation. Radiative recombination of an electron–hole pair in the quantum dot consequently reveals information on the quantised energy levels and the optical selection rules. Therefore, micro-photoluminescence (μPL), i.e. measuring the spectrum of QD light emission under continuum excitation, has been an essential workhorse of quantum dot research over the years.

In a typical μPL setup, a schematic can be found in Figure 6(*a*), Section 3.1.3, laser light is directed by a beamsplitter to an objective which focuses the light onto the QD sample (the triangle in the illustration). The numerical aperture of the objective and the laser wavelength determine the focal volume the laser excites. The luminescence emitted from the sample is collected by the same objective and is directed through a pinhole (RP in the illustration). The function of the pinhole is to limit the sample volume from which luminescence is collected. Selection of the objective numerical aperture and pinhole diameter result in diffraction limited focal volumes of less than 1 μm^3 which, provided the sample density is low enough (1–10 dots per μm^2), can enable single QD spectroscopy. After the pinhole, a flip mirror (FM in the illustration) directs the luminescence to an imaging spectrometer that is able to resolve the spectral content of the luminescence.

We present in Figures 4(*a*) and (*b*) two of the first reported ensemble and δ-function-like spectra of photoluminescence from InAs/GaAs quantum dots [8,9]. Figure 4(*a*) displays the broad emission of a QD ensemble at the low energy tail of the spectrum along with the sharper bulk luminescence at 1.38 eV. In the measurements presented in Figure 4(*b*), to probe

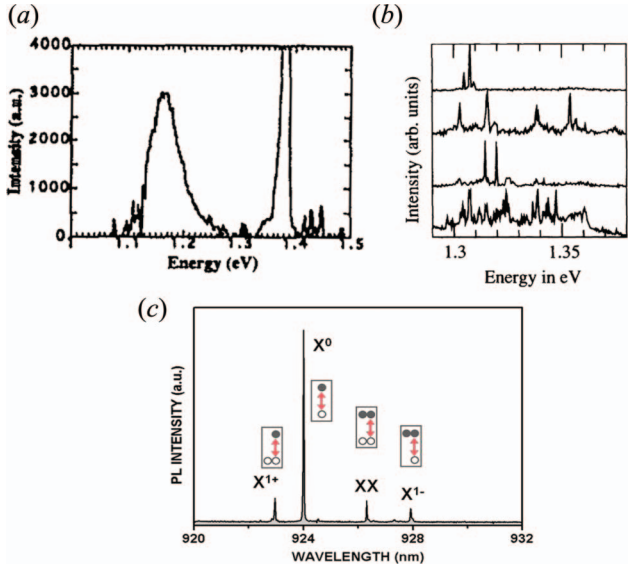

Figure 4. (*a*) Photoluminescence from ensemble of InGaAs QDs [8]. (*b*) Top three traces are μPL spectra recorded from three different sample locations at 10 K. The bottom trace is the sum of 20 spectra [9]. (*c*) μPL from a single well-isolated InAs QD showing the individual transitions. The solid circles represent electrons and the open circles are holes.

individual QDs the sample surface was etched to contain small mesas separated by 15 μ m. The mesas limited the spatial region of excitation and collection revealing signatures of single QD emission although the sample density resulted in $\sim$250 QDs within the diffraction limited collection spot size. The etched mesa is similar in effect to an appropriately selected pinhole placed in a conjugate image plane of the microscope. Figure 4(*c*) is a similar μPL measurement on a well-isolated single InAs QD displaying the individual optical transitions with the corresponding charge configurations.

3.1.2. Exciton lifetime – time correlated photon counting

Although photoluminescence is able to determine the transition energies between optically active quantum dot electronic states, it is not able to associate a time scale with these transitions. Assuming a stable ground state, it is natural to invert the linewidth measured with the spectrometer to obtain the transition timescale. Unfortunately, for most QDs and a single spectrometer, the transition linewidth is narrower than the instrument's spectral resolution (a typical resolution is 30 μeV), hence numerous publications historically have used the term *resolution-limited emission* over the years. It is clear from these considerations that in order to assess the dynamics of the light emission process a new technique is needed – one with temporal resolution.

One approach with temporal resolution is to generate an ensemble of electron–hole pairs in the surrounding matrix by a short nonresonant laser pulse, typically on the order of a few hundred femtosecond to a few picosecond duration. In bulk semiconductors with direct bandgap, excitonic lifetime is on the order of a few picoseconds. When confined in all three spatial dimensions, as in a quantum dot, the lifetime of excitonic complexes is enhanced by about three orders of magnitude. Due to the unequal recombination rates of excitons in extended versus confined systems, only the excitons captured by the quantum dot remain even after a mere tens of picoseconds following the initial excitation pulse. This allows the quantum dot exciton to decay in the absence of any other excitations, and thus free from excited carrier induced effects. QD emission, spectrally filtered from all other excitonic recombinations, can then be detected by photon counting photodetectors. A registry of photon arrival time delays with respect to each excitation laser pulse thus builds up a temporal histogram of detection events. This histogram can be interpreted as the probability that a QD exciton remains alive (or QD remains in the excited state) over a timescale.

Figure 5 presents data from a single InAs QD measured as a function of average pulse power for a 3 ps wide excitation pulse [10]. At the lowest pump power (bottom curve), the exciton (or excited state) lifetime is revealed, and the fit decay time is 0.8 ns. For an ideal two-level system, such a measurement will produce a single exponential decay of width directly related to the excited state lifetime, and thus the natural linewidth of the transition through a Fourier transform. As the average pulse power is increased, there is a pronounced shift in the start time for the exciton decay. This is in fact a very nice signature of multi-excitonic effects taking place at high pump powers. The probability of capturing one exciton is already high, so an additional exciton capture within the recombination time becomes considerable. Consequently, exciton decay is necessarily delayed by the characteristic biexciton decay time. It is important to note here that not only the radiative decay, but also any other process that results in exciton population loss will affect this histogram. For example, if there is a nonradiative channel for exciton decay that is larger than the radiative lifetime, the measured histogram may exhibit a double exponential where the decay of each exponential is dictated by the radiative and nonradiative decay rates. Quantum dot systems, such as CdSe/ZnS core/shell colloidal QDs, do possess finite nonradiative decay rates [11], where one mechanism leading to nonradiative decay in CdSe/ZnS is Auger recombination – a process whereby an exciton pair recombines to form a more energetic electron. In the case of InAs QDs with effectively no appreciable

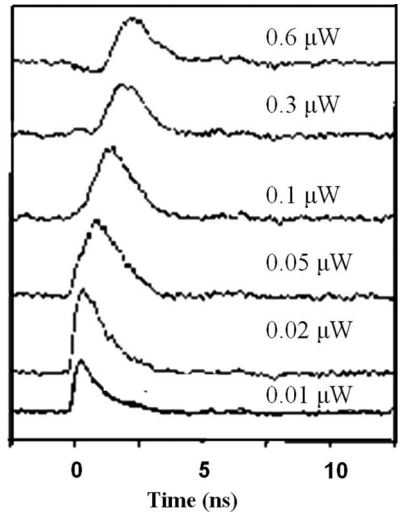

Figure 5. The photoluminescence intensity from a single InAs QD, at 20 K, as a function of time after excitation with a 3 ps laser pulse. The inset indcates the average power for the excitation pulse. The lowest power decay curve fits to an excited state lifetime of 800 ps [10].

nonradiative decay channels, another mechanism does lead to biexponential decay in lifetime measurements – bright and dark exciton mixing. A clear study of this effect can be found in [12,13].

3.1.3. *Two-time field and intensity correlations*

Time-correlated photon counting allows us to measure the emission timescale of the photons, but reveals very little about their coherence properties. In order to understand the extent of excitonic and carrier induced decoherence mechanisms taking place prior to or during the exciton recombination, we need to use a technique where the signal is directly linked with the degree of coherence of the QD emission. A first step to quantify the degree of coherence in the emitted photon stream is to interferometrically measure two-time field correlations, where temporal correlations in the light beam are revealed by interfering the field with its time delayed replica. One approach, illustrated in Figure 6(*a*), is to use a Michelson interferometer which maps path length difference between the two interferometer arms to time delay. Mathematically, this can be represented as

$$I_D(\Delta x) = 2 \times I_{\text{avg}}(1 + \Re[g(\Delta x)]), \tag{2}$$

where

$$g(\Delta x) = \exp(-\mathrm{i}2k\Delta x - 2\gamma|\Delta x|). \tag{3}$$

Δx is path length difference between the two arms of the Michelson interferometer and γ is the total damping rate of the transition (we have assumed the transition lineshape is Lorentzian). In Equation (2), I_{avg} is the average intensity that reaches the detector. While the first term in the parentheses of Equation (2) reveals the average intensity of light and does not exhibit relative optical path length dependence, the second term, in Equation (2), modifies the detected signal to the extent that the parts of the optical field at two different times remain correlated. Figure 6 presents this measurement on photons emitted from a single self-assembled indium phosphide QD [14]. In Figure 6(*b*) widefield images of QD emission are presented for the open circles decorating the interferogram in Figure 6(*c*). The decay of the interferogram envelope for large path length differences, Figure 6(*d*), reveals the damping rate γ defined in Equation (2) will result in an exciton with an emission linewidth of 186 μeV. The inverse of this quantity yields the coherence time of the emitted photons. Zwiller et al. indeed extract a coherence time of 140 ps, much shorter than the measured excited state lifetime of 1.2 ns, allowing for an accurate quantification of the

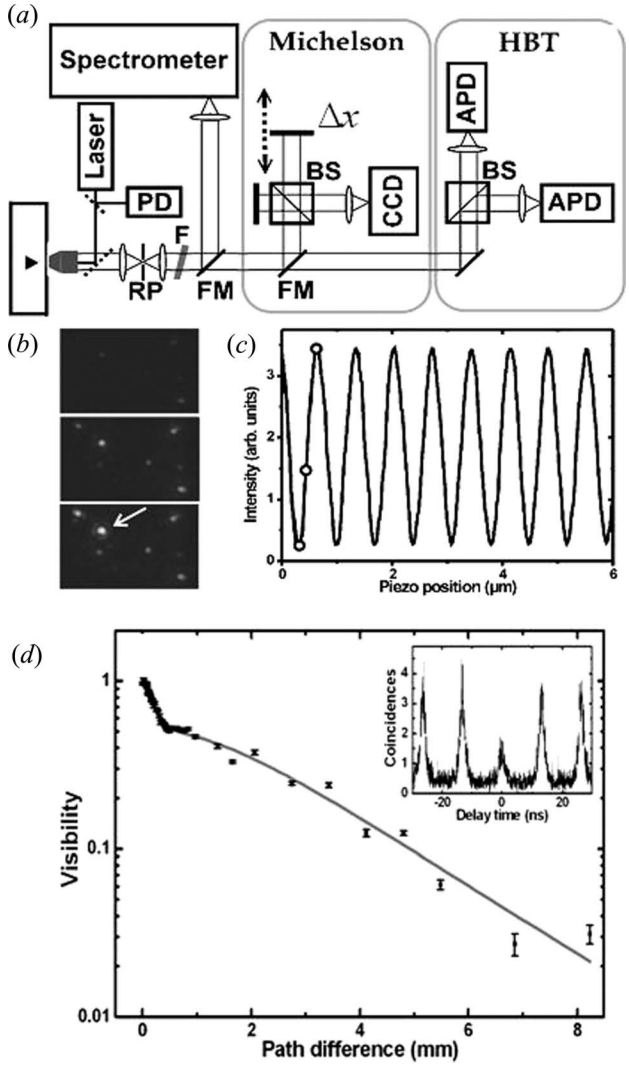

Figure 6. (*a*) Experimental setup. Flip mirrors (FM) are used to direct the emitted photons to either to a spectrometer, to a Michelson interferometer, or to a Hanbury-Brown and Twiss correlator. The latter two are built around nonpolarising beam splitters (BS). A removable pinhole (RP) can be used to select a single dot. A narrow bandpass filter (F) is tilted to transmit single spectral lines. (*b*) Images taken through the Michelson interferometer showing several dots with varying intensity as the mirror is scanned. (*c*) Single-dot photoluminescence intensity for the dot marked by an arrow in (*b*) as a function of mirror position. The circles indicate the three positions where the images were taken. (*d*) The envelope of the exciton emission interferogram measured at 6 K with a 5 mm relative path difference between the two arms. The inset is the intensity correlation, $g^{(2)}(\tau)$, measurement on the same exciton [14].

dephasing mechanisms. One notable source of dephasing in this measurement is the optical charging of the QD environment that results from above bandgap nonresonant excitation. Specifically, photoexcited electron hole pairs, a portion of which relax to occupy the QD exciton states, may also become trapped at defect

sites in the vicinity of the QD. These local charges create a varying Stark field (uncontrolled electric field at the location of the QD) which acts to shift the QD transition energy. If the time-scale of the measurement samples a number of local defect charge configurations then the QD transition energy will shift throughout the course of the measurement. The shift in the energy will act to smear out the single-photon interference fringes and will lead to a reduction in the measured contrast, i.e. extracted photon coherence time.

Two-time measurements can also be carried one order higher, where the correlations in optical intensity rather than the field are considered at two different times (in Figure 6(*a*) the HBT box). In this case, the signal arises due to intensity fluctuations and does not depend on interference or phase relations within the fields. Therefore, historically second-order correlations of strong light beams were obtained from correlating photodetector current outputs $i(t)$ after detection, in the form of

$$g^{(2)}(\tau) = \langle i(t)i(t+\tau)\rangle / \langle i(t)\rangle\langle i(t+\tau)\rangle\,. \qquad (4)$$

A truly uncorrelated pair of photocurrent measurements gives unity value for this function, and any departure from unity value indicates correlation (or anti-correlation) within a characteristic memory time-scale of the source. Consequently, Equation (4) can be written in the form $g^{(2)}(\tau) = 1 + \eta C(\tau)$. For intense optical beams detected by photodiodes, the registered current is proportional to the intensity, therefore the second-order optical correlations are mapped conveniently to the current. The scenario is quite similar for single photon light levels where a temporal registry of individual detection events carries similar correlations to the incident photon stream. For example, coherent light (such as laser emission) exhibits no correlation ($\eta = 0$) and $g^{(2)}(\tau) = 1$ for all delay times whereas the memory present in single photon emission from a two-level system results in anti-correlation, $g^{(2)}(\tau) < 1$ with $\eta = (-1)$ and $C(\tau) = \exp(-\gamma|\tau|)$. In order to perform second-order correlation measurements on single QD emission lines, the Hanbury-Brown Twiss (HBT) experimental arrangement, shown in Figure 6(*a*), is used. The collected QD emission is split to be detected by two photon counting detectors. Photon detection times are then registered per detector. A count is recorded conditioned on the previous detection of a photon – a coincidence count. A histrogram of counts is plotted as a function of the delay time between successive detection events using time–amplitude conversion. Figure 7 shows intensity (photon) correlation measurements performed on the emission under nonresonant excitation for an ensemble of InAs QDs (panel 1) and two individual InAs QDs (panels 2/3)

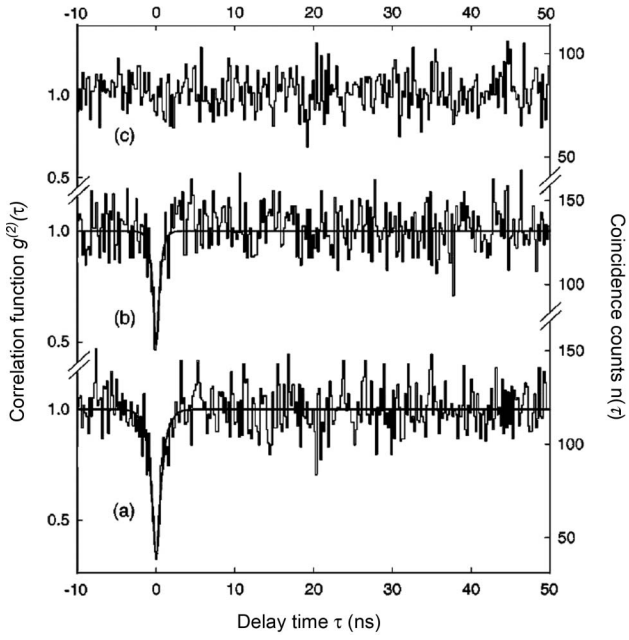

Figure 7. The data presents the measured distribution of coincidence counts and a fit of the correlation function. Panel 1 is for a high density QD sample with more than one QD emitting within the focal volume of the collection optic. The measured $g^{(2)}(\tau)$ does not exhibit antibunching. Panels 2 and 3 are for a single InAs QD at two different pump powers. Panel 2 (3) is taken at 125 W cm^{-2} (66 W cm^{-2}). Panel 3 exhibits a pronounced antibunching dip [15].

[15]. The pump power in panel 2 (3) is at the onset (below) the power necessary to saturate the QD emission. In panel 1, there is no correlation in the photon emission from the ensemble of QDs, and there is no deviation from unity as a function of delay time. Panels 2/3 show that the detector outputs are uncorrelated in all time scales except around zero time difference, where detection events are anti-correlated. The QD emission therefore is antibunched, or has a degree of temporal order. This is a consequence of the anharmonicity of the energy levels involved in the QD emission. In these systems only one photon can be generated within a radiative lifetime. Therefore, the two-time dependence of coincidence counts also reveals the temporal profile of photon emission. For a two-level system with Lorentzian spectrum, with a linewidth of γ, we expect to see an exponential decay in the time domain, and photon correlation measurements indeed reveal a symmetric double exponential profile. It is important to note here that this technique measures the probability of two-photons being generated sequentially, therefore it is immune to deviations from ideal configurations. For example, if the experimental setup includes imperfect elements or has mechanical instability, parameters

extracted from an interference-based measurement would be significantly affected, but not the observed photon correlation function. Alternatively, we might be dealing with less than ideal atomic-like states where pure (elastic) dephasing and nonradiative decay mechanisms of the excited state may be non-negligible. While previously discussed lifetime measurements would only provide the *total* excited state decay characteristics, photon correlation measurements, provided the excitation method can be classified as incoherent, will reveal only the *radiative* part and remain immune to all other decay and dephasing channels [16]. In experimental physics such power comes rarely from such a simple arrangement. Another point we wish to emphasise here is that while two-time correlation measurements to date have been performed using two independent detectors, identical measurements could also be performed using a single detector with sufficiently fast response and timing capability. Therefore, there still is a lot of attention on the development of single-photon sensitive, photon-number resolving and high temporal resolution detector technology [17], where superconducting detectors seem to offer promising capabilities for this direction [18].

The power of photon correlation measurements does not stop here at single photon generation, and can reveal a lot more about the internal dynamics of multi-exciton recombination. We have seen previously that the individual recombination processes of neutral and charged excitons as well as biexcitons have well distinguished energy shifts (see Figure 4(*c*)) and have already seen such consequences on lifetime measurements (see Figure 5, top panel). Therefore, the intensity correlations between any two QD emission lines can be measured as well. Figure 8 shows such measurements for biexciton–exciton cascade decay [19]. The breakdown of symmetry around the zero time delay between coincident detection events reveals the one-sided ordering of the cascade process. The probability to detect exciton decay is increased on the condition that a photon from biexciton decay has been detected, while the probability to detect a photon from biexcitonic decay is essentially nil upon detection of a photon from exciton decay. This technique therefore gives direct information on the emission time ordering, plays a crucial part in identification of the observed spectral lines and allows us to identify metastable intermediate states during the cascade.

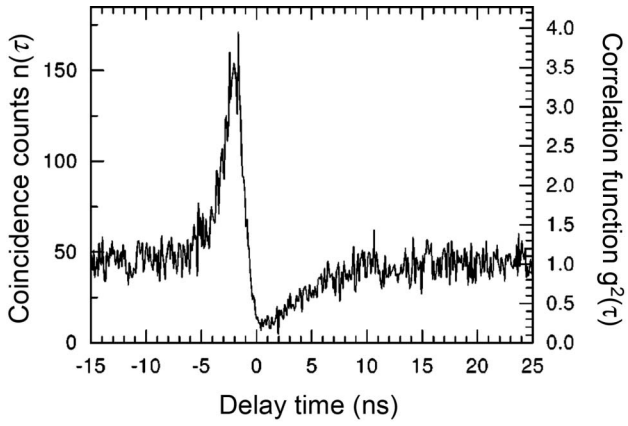

Figure 8. Cross-correlation of the biexciton–exciton cascade emission. The experimental apparatus is identical to Figure 6(*a*) except the detection of the exciton emission is conditioned on the measurement of biexciton emission. To realise this experimentally, narrow band spectral filters (1–2 nm FWHM centred on either the exciton or biexciton emission line) are placed in front of each APD [19].

3.2. *Optics of quantum dots: resonant excitation*

Techniques presented in the previous section can give valuable information on exciton capture and decay dynamics as well as properties of the generated optical fields. A common feature in all of these studies is the incoherent pumping of the quantum-dot transitions through carrier generation in either the host matrix such as GaAs or the quasi-continuum states above the higher-lying confined states of the quantum dot – what we have termed nonresonant excitation. This excitation method leads to photon-emission-time jitter, since it relies on an uncontrolled relaxation step to populate the excited exciton state, and spectral wandering of the quantum-dot transition larger than the transition's linewidth due to optical charging of the host semiconductor matrix. Both effects reduce the usefulness of non-resonantly generated single photons in linear-optics quantum computing algorithms, even if the quantum dot is coupled to a cavity [20]. In an attempt to both address this previous shortcoming and provide spectrally selective access to the quantum-dot electronic transitions, increasing attention has turned to resonant optical excitation. Noting all successful quantum-information science (QIS) implementations on well-developed qubit candidates, such as trapped ions, have relied on resonance scattering, it is clear that resonant optical control of QD transitions is desirable. In the realm of resonant spectroscopy, we make a further distinction between temporal and spectral measurements.

3.2.1. *Temporal measurements*

A single ultrafast pulse propagating through a material may be affected by both absorption and dispersion. Transient nonlinear optical spectroscopy, also known as pump–probe spectroscopy, involves a sequence of ultrafast optical pulses, which are separated in time

and tuned to the spectral vicinity of an absorption band in a material. Conditional on the optical excitations or an induced polarisation field due to the first pulse (usually called the pump) the propagation of the second pulse (i.e. the probe) may show a deviation from what one would expect from the single pulse case. Therefore, a dynamical response from the material can be mapped out based on the time delay between the pump and probe pulses. The selection of the laser pulse spectral/temporal width depends on the desired experiment, but typical considerations for QD excitons are the timescale of the dynamics limiting the pump–probe delay and the spectral separation of other excitonic resonances limiting the pulse bandwidth. The pulse spectral width (via Fourier transformation) dictates the shortest temporal separation between two pulses and consequently sets the experiment's temporal resolution. Before continuing we highlight that nonlinear spectroscopy techniques result in weak signals (typically 15 orders of magnitude with respect to the excitation pulses) and the measurement of these small signals presents an experimental challenge [21]. A first step toward signal recovery is to interfere the signal field on the detector with a local oscillator field that is either derived from a reference pulse that does not interact with the QD or with one of the excitation pulses. Mixing the signal field with a second field on a photodiode is referred to as heterodyne detection, a term borrowed from radio wave engineering. The advantage of heterodyne detection is that the interference term depends on the signal amplitude multiplied by the conjugated strong local oscillator field amplitude and this acts to amplify the measured signal. In addition to interference it is common to modulate the excitation pulses so that the signal is carried by distinct spectral components in the measured photocurrent which can then be accessed with a phase-sensitive lock-in detection system.

Within the family of pump–probe techniques used for ensemble and single QD spectroscopy, there is a particularly elegant and powerful modality, where the pulse sequence itself generates a third-order nonlinear polarisation in the QD which acts as a source of an additional field that carries information related to the dynamics of the QD excitons. This polarisation field oscillates at a set of frequencies determined by central frequencies of the two laser pulses including a beat frequency, and, if the pulses are non-collinear, the generated field may even propagate in a distinct direction due to the phase matching requirement of the involved k -vectors. This counter-intuitive response to a two-pulse sequence can be seen in the relevant density matrix equations of motion coupling populations to coherences for spectrally shifted excitation pulses [22].

In the context of QD spectroscopy the initial motivation for two-pulse degenerate transient FWM was to circumvent the inhomogeneous broadening inherent in ensemble QD measurements, and directly access the dephasing time of a single QD exciton. In this spectroscopy modality the central frequency ω_0 of a laser pulse is tuned to the mean frequency of the ensemble X^0 exciton resonance. As can be seen in Figure 9(*a*), the exciting laser pulse is split into three parts – a pump, a probe and a reference pulse. A controllable time delay, τ_d, is established between the pump and probe pulses. The pump (indexed with a 1) and probe (indexed with a 2) pulse each receive a small, but distinct, frequency up-shift typically with acoustic optic modulators to $\omega_1 = \omega_0 + \omega_{RF1}$ and $\omega_2 = \omega_0 + \omega_{RF2}$. The pulse pair is subsequently directed to the QD sample exciting a third-order polarisation. It is at this point, when the pulses excite the sample, where there are two variations in implementing FWM. In [23] the time-delayed pump pulse and probe pulse illuminate the sample with well-defined non-collinear k-vectors, k_1 and k_2, where the general scheme is nicely illustrated in Figure 9 [24]. The resultant polarisation radiates in a direction determined by the wavevector combination $2k_2-k_1$ and oscillates with a frequency $2\omega_2-\omega_1$. The subsequent source field (resulting from the QD nonlinear polarisation) is mixed with a reference laser pulse still at ω_0, but delayed by time τ_r, on a photodiode. A phase-sensitive lock-in amplifier demodulates the FWM signal in the measured photocurrent at $2\omega_{RF2}-\omega_{RF1}$, which is typically in the tens of MHz frequency range.

Another approach to FWM, which does not exploit the additional wavevector selectivity afforded by the previous approach, is presented in [25]. Again the pump and probe pulse are time delayed, but instead of illuminating along fixed, non-collinear, directions the collinear pump and probe pulses are focused by a high numerical aperture objective onto the sample as illustrated in Figure 9(*b*). The induced nonlinear polarisation radiation is collected by a similar objective and mixed with the reference pulse directly on a photodiode. Unlike the previous example where the signal was free from pump and probe pulse background, this second approach relies entirely on the lock-in amplifier to distinguish the signal of interest from the background pulses, which still modulates the photocurrent at a frequency $2\omega_{RF2}-\omega_{RF1}$. The stringent k -vector considerations are not an issue for this modified version, at the expense of reduced sensitivity in detection. Although these two modalities are slightly different with respect to signal acquisition, both benefit from the essential advantage of the transient FWM signal; its immunity to inhomogeneous broadening. Inhomogeneous broadening is an inherent

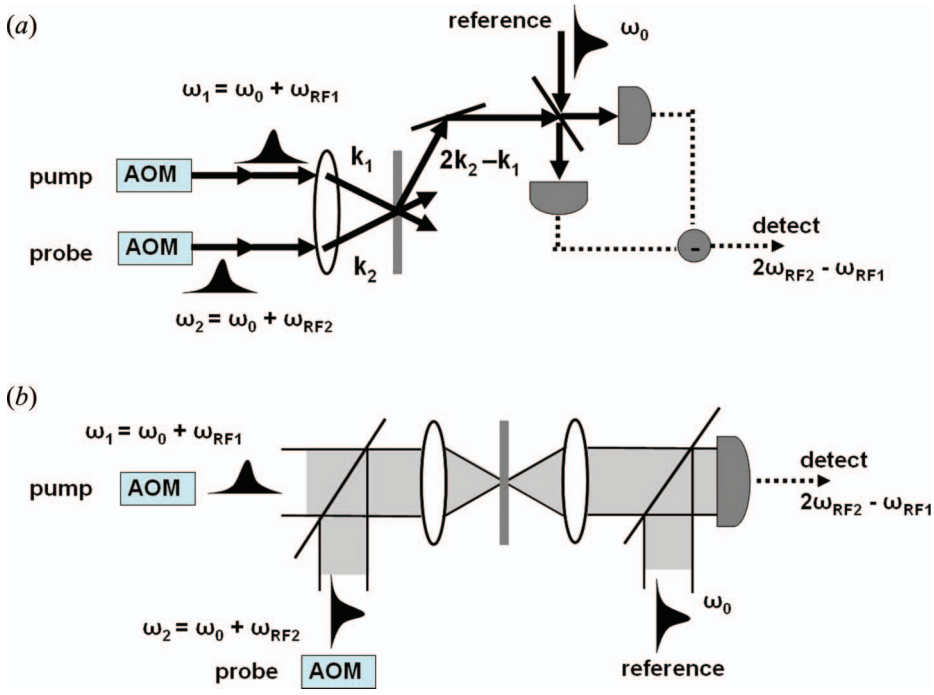

Figure 9. Schematics of the setups for the two four-wave mixing modalities. (*a*) A pump and a probe pulse, at two distinct frequencies, illuminate the sample along two directions. The phase matched signal, in a direction distinct from the pump and probe, is mixed with a reference pulse on a photodiode. A lock-in amplifier demodulates the signal, at a frequency $2\omega_{RF2}-\omega_{RF1}$, from the photocurrent. (*b*) Same as (*a*) except the pump and the probe pulses are now focused and collected by high numerical aperture objectives.

feature of QD emission spectra in high density QD samples (when there are a number of optically active QDs within the microscope focal volume) as a result of the QD size distribution. Specifically, when the inhomogeneous spectral broadening of the ensemble is considerably larger than the homogeneous dephasing rate of a single QD exciton, the polarisation will radiate a light pulse at exactly 2 times the pump–probe delay; the photon echo. Figure 10(*a*) presents the measured echo pulse as a function of the probe delay τ_d from an ensemble of InAs QDs at a temperature of 50 K. The important information is obtained from plotting the integrated area of this light echo pulse as a function of pump–probe delay. The strength of the photon echo generated depends on the coherence of the ensemble, so the decay of the integrated area is determined by the total dephasing rate of a single QD exciton. Figure 10(*b*) is an example of the integrated echo pulse area FWM signal. The extracted dephasing rate of 630 ps when this measurement was repeated at 7 K was the first of its kind to suggest the excited state decay was predominantly the result of radiation broadening.

The second transient nonlinear spectroscopy technique we describe is degenerate pump–probe

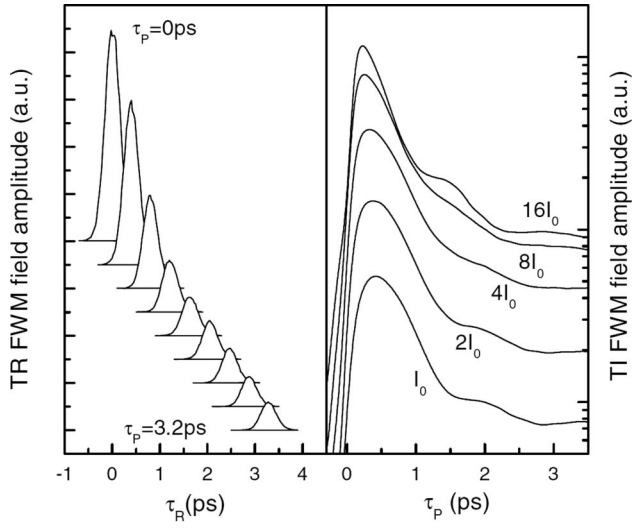

Figure 10. Time resolved four-wave mixing data from an ensemble of InAs QDs at 50 K. (*a*) The echo pulse as a function of the reference pulse time delay τ_r. The time delay between the exciting pulse pair is varied in 400 fs steps from 0 to 3.2 ps. (*b*) Time-integrated four-wave mixing obtained by integrating the echo pulse area in (*a*) at different excitation intensities. (*a*) Corresponds to the $2I_o$ trace in (*b*). Exponential fits to the traces in (*b*) yield the dephasing time of a single QD exciton transition [25].

spectroscopy. Just like FWM, pump–probe also interrogates the induced third-order polarisation, but, in contrast to FWM, the pump–probe signal is derived from the polarisation's response at the probe field's frequency. Consequently, this alternative technique probes essentially the occupation probabilities of the excitonic states rather than being limited by their coherences. In other words, the previous FWM signal (at the beat frequency of $2\omega_{RF2}-\omega_{RF1}$) will vanish if the coherence between the two states of the transition is lost, while the probe response (at the probe modulation frequency ω_{RF2}) will still be visible as long as the excitations are present, much like the lifetime measurements discussed before. The two pulses are delayed in time by τ_d, but now the signal field is mixed with the probe field on the photodiode. A lock-in amplifier filters the measured photocurrent isolating the signal at a frequency ω_{RF2}. In a pump–probe experiment the probe pulse transmission as a function of delay time τ_d is a direct measure of the excited state lifetime: both radiative and nonradiative contributions. A further twist on the pump–probe technique results from plotting the probe transmission at a fixed delay time τ_d as the pump and probe centre frequency are varied in unison. In this case the time-domain technique is able to unmask frequency domain information and probe the absorptive resonances of the QD. An example of the measured data in these two approaches is in Figure 11 for a single GaAs interfacial (fluctuation) QD [22]. In the top panel in Figure 11(*a*) two co-polarised 6 ps wide pulses, with a fixed 6 ps delay between the pulses, illuminate the sample. The absorption of the probe pulse, the transient differential transmission, is plotted as a function of the two pulses' centre frequency. The peaks in the absorption data reveal electronic transition energies in the QD. Figure 11(*b*) is the measured probe pulse area as the delay between the pump and probe pulse is varied. The measured excited state decay time is 41 ± 2 ps. Finally, the lower panel in Figure 11(*b*) presents differential transmission with a continuous wave (CW) laser. The narrowband CW laser greatly improves the spectral resolution of the absorption measurement, and as we will see in the coming section, has become an indispensable tool for selective excitation of QD transitions.

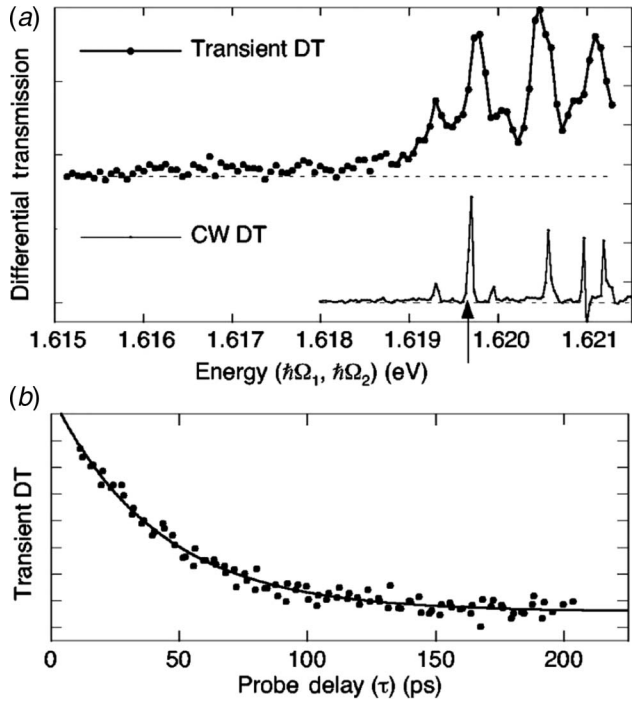

Figure 11. Degenerate pump–probe spectroscopy data. (*a*) Copolarised pump and probe pulses with widths of 6 ps are delayed by 6 ps and the transmission is measured as the pulse centre frequency is varied. The dashed line is the zero signal level. In the lower panel, a cw laser is tuned through the QD resonance. We will focus on the merits of this technique in the next section. (*b*) The integrated probe pulse signal as a function of its delay from the pump pulse. The fit exponential decay reveals an excited state lifetime of 41 ± 2 ps [22].

3.2.2. *Spectral measurements*

We introduced fundamental transitions per charge configuration in the quantum dot in the first section (see Figure 3). The purpose of photoluminescence measurements was to map out the spectrum of all allowed transitions due to various charge combinations. Given a typical resolution of 30 μeV, this appears insufficient for resolving spin and anisotropy induced fine structures. Likewise, even when the ground state of the quantum dot is controlled to be in a particular charging configuration, we introduced nothing to prevent the capture of uncontrolled charge combinations under above-band-gap excitation. Therefore, while this particular type of excitation allows for mapping out the optical transitions, it still renders any systematic access to individual spin states impossible. Pump–probe techniques allow for precise measurement of the excitonic dynamics, but due to the extended bandwidth of the optical pulses, frequency selectivity of individual transitions within the fine structure is limited. In order to address this shortcoming, an alternative technique is utilised where temporal resolution is sacrificed for such spectral selectivity. Ultrafast pulse pairs are replaced by one or more highly monochromatic single transverse and longitudinal mode lasers with tuneable optical frequencies. We can now address a transition of interest directly and selectively among many allowing us to

study features such as optical selection rules and oscillator strengths by observing the scattered laser light.

The signal in this case is still due to the interference of the background laser and the scattered dipole radiation, where the transmitted laser field is measured by photodetectors rather than the emitted photons being detected by a spectrometer. If the laser field is in resonance with a quantum dot transition, the optical field scattered by the quantum dot interferes with the background optical field. The total field observed upon transmission through the quantum dot includes the signature of the quantum dot response to the light field. All measurements are performed in the far-field so the phase difference is a result equivalent to the overall Guoy's phase acquired by the background laser. Consequently, we typically measure the absorptive response directly in intensity change. In short, the measured optical field intensity will trace out the following response:

$$I(\Delta)/I(\infty) = 1 - \alpha_o\left[(\Gamma^2/4)/(\delta^2 + \Gamma^2/4)\right], \qquad (5)$$

where α_o is the effective absorption strength determined by the laser focus area and the quantum dot oscillator strength and is typically in the range of $10^{-3}-10^{-2}$. In order to see this response one has to have control over the detuning δ and this can be achieved in two ways: either by sweeping the optical frequency of the excitation laser with respect to the QD transition or by shifting the quantum dot emission energy via DC Stark effect through an external electric field.

Unlike photoluminescence measurements, the signal strength here with respect to the background laser intensity is usually on the order of 10^{-3} as dictated by α_o and lock-in based detection is required in order to eliminate this background. The modulation required for the lock-in scheme is obtained by electronically modulating the external electric field with a square wave signal. Normalising by the total power at the photodetector one can calculate the deviation of the transmissivity from the off-resonant value $\Delta T/T$. This is called Stark-shift modulation spectroscopy and further experimental details of this technique can be found in [26]. Given that we are no longer limited by the spectrometer spectral resolution of 30 μeV, but rather the uncertainty of the applied gate voltage and the spectral bandwidth of the applied laser, resonant scattering has significantly higher resolution, on the order of 0.04 μeV. The previously predicted fine structure of each optical transition can now be observed clearly, as displayed in Figure 12(*a*). The black (grey) data set is obtained with a π_X (π_Y) linearly polarised

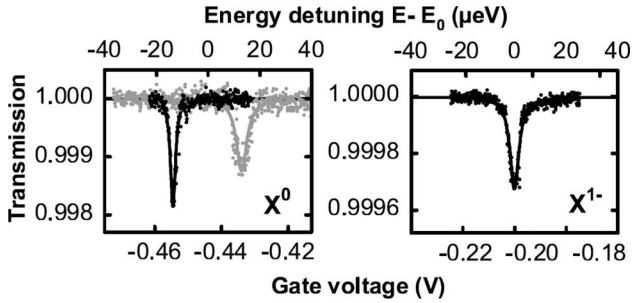

Figure 12. Differential transmission data for the neutral exciton (left panel) exhibiting the fine structure $x-y$ splitting, in this case 27 μeV, due to the electron–hole exchange. Differential transmission data for the trion exciton (right panel). The exchange splitting observed in panel (*a*) is zero since the electrons are in a spin singlet [27].

laser. Figure 12(*b*) is the same measurement on X^{1-} displaying a single peak due to degeneracy [27]. Taking advantage of this high spectral resolution, QD transition linewidths on the order of 1.3 μeV have been observed [28]. In addition, this response can in addition be controlled to yield both absorptive and dispersive lineshapes [29] depending on the relative phase between the laser and the QD scattering field. Nevertheless, the relatively modest signal to background level limits how fast this measurement can be completed. However, recent advances incorporating solid immersion lens technology [30] showed that the measured signal strength can be increased further leading to higher detection bandwidth [31,32].

4. Recent achievements utilising these techniques

What we have presented so far is a survey of optical techniques utilised in the quantum dot research in the broad sense. While each technique presents a complementing side to complete spectroscopy of quantum dots, some have in parallel been utilised to perform some key achievements. In this context, quantum information processing has benefited significantly from the re-interpretation of spectroscopic concepts and measurements. We give below a handful of examples along these lines, but emphasise that we are leaving out a vast area of quantum dot research on conventional optoelectronics technology, such as lasers and optical switches.

4.1. Deterministic source of single photons and quantum cryptography

One of the earliest applications of quantum information science was quantum cryptography, which drew its power of security from the indivisibility of a single photon. The information (the bit) is encoded on single

photons thus 'tapping' the quantum channel was quantum mechanically forbidden. The lack of a true single photon source prevented the use of the no-cloning principle, and had to revert once again to the 'difficulty' of eavesdropping by using either heavily attenuated laser beams with average photon number much less than one, or down-conversion processes that generate photon pairs with a small probability of generating multiple photon pairs in well determined directions. Sacrificing one of the photon pairs in down-conversion for timing gives a sense of heralding to the photons in the other direction, but the probability to have more than one photon in a pulse still remains finite. A compact, stable, reliable source of single photons was the missing link for relying on quantum mechanical principles for ultimate cryptographic security rather than assumed difficulty in practice of breaking the cryptographic code.

We have discussed how intensity (photon) correlation measurements reveal the decay dynamics of the excited states in quantum dots. In 2000, two groups reported one of the first applications of this technique in the realm of quantum information for the realisation of deterministic heralded single photon generation [33,34]. In these works, the above-bandgap nonresonant continuous-wave excitation laser was replaced by an ultrafast laser pulse train which generated excitons, in the vicinity of a quantum dot, at well known times. After each excitation pulse, a high density of photo-excited excitons was to ensure the probability to capture at least one exciton inside the quantum dot approached unity. While the number of excitons captured inside a quantum dot is statistically varying, the distinct exciton emission wavelengths due to Coulombic interactions allows one to spectrally filter out only the neutral exciton recombination. The result is a single photon generated with unity probability at a well-defined wavelength, at discrete times manifested by the excitation laser pulses. Figure 13(*a*) displays the photon correlation measurement under these conditions. Unlike the continuous-wave excitation profile, we see uniform coincidences only at discrete time delays indicating that the emission comes as a pulse train following the excitation laser pulse train. The absence of the central coincidence peak is due to the lack of another photon emitted simultaneously at

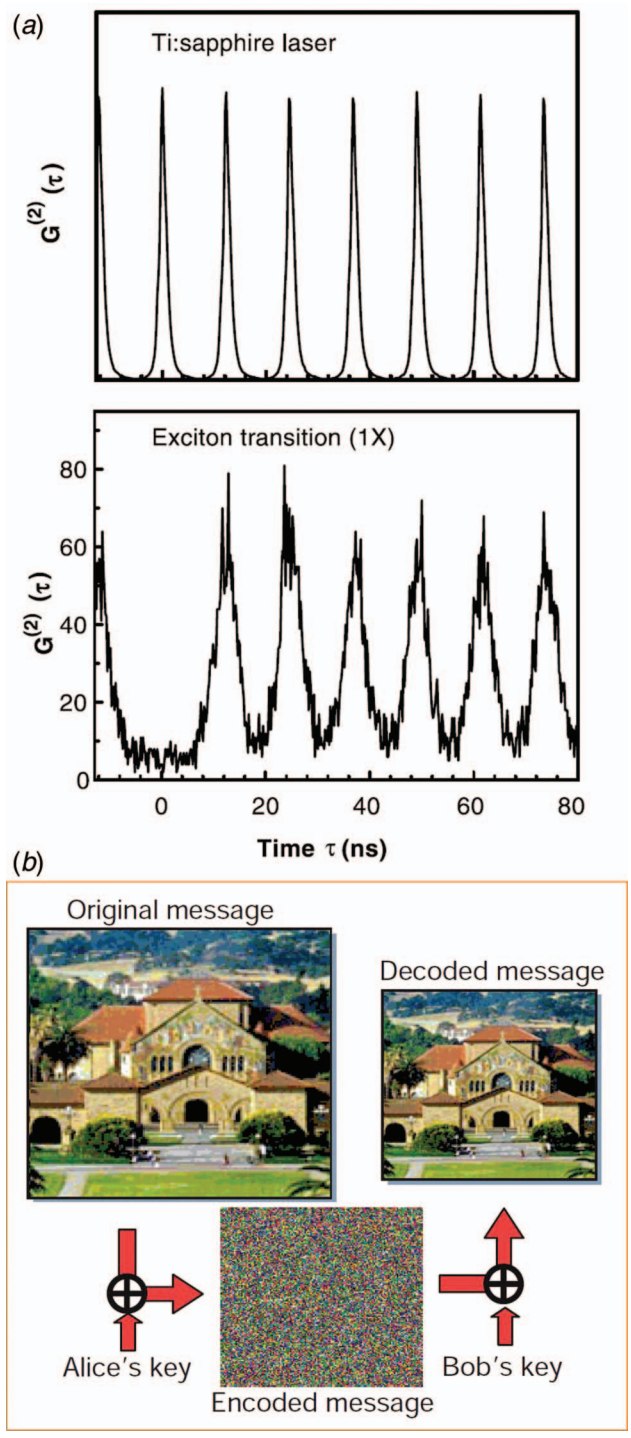

Figure 13. (*a*) The top panel is the autocorrelation of a 250 fs Ti:sapphire laser and the bottom panel is the autocorrelation of single photons emitted from the ground state exciton of a QD embedded in a microdisc cavity under pulsed excitation. In the bottom panel (in contrast to the top panel), the zero delay time is nearly zero. This is a result of the QD emitting one photon at a time. More importantly, upon pulsed excitation, the QD emits a single photon in well-defined time bins – the so-called photon turnstile [33]. (*b*) The polarisation of single photons emitted by a QD based photon turnstile is used exchange a secure key between Alice (the transmitter) and Bob (the receiver). The key is used to encode and decode a 140 × 141, 256 pixel colour bitmap of the Stanford University's memorial church (the top image). The encoded message appears as white noise to all parties that detect the encoded photons without the key except for Bob who has the correct key [35].

the same wavelength, verifying the single photon nature of this heralded emission process.

In 2002, Santori et al. implemented the first quantum key distribution protocol using a single quantum dot as a true single photon source [35]. Figure 13(*b*) shows the original and decoded image when the polarisation state of individual photons emitted from a quantum dot are used to exchange the key necessary to decode the image.

4.2. *Going beyond single photons: polarisation entangled photon pairs*

A cascade two-photon emission process with intermediate level degeneracy was the source of entangled photons for the seminal work by Aspect et al., where $J = 0 \rightarrow J = 1 \rightarrow J = 0$ type cascade decay of Calcium atoms was used for the first experimental demonstration of bipartite entanglement and violation of local realism models for quantum theory [36]. Once the analogous cascade nature of the biexciton-exciton decay in quantum dots was revealed, the route to generation of frequency and polarisation correlated (or entangled) two-photon states was established. The two-photon field emitted via the biexciton–exciton cascade decay process, illustrated in the inset of Figure 14(*a*), can be written as

$$(|\omega_1 H_{XX}, \omega_2 H_X\rangle + |\omega_3 V_{XX}, \omega_4 V_X\rangle)/2^{1/2}. \qquad (6)$$

This is a maximally entangled state in the strict sense of the word. However, revealing the degree of, for example, polarisation entanglement would be burdened by the simultaneous frequency entanglement. The frequency tag on the decay channel comes from the electron–hole exchange (discussed previously in relation to Figure 12), labelled S in the inset of Figure 14(*a*), which lifts the double degeneracy of the intermediate X^0 excitonic energy levels. Therefore, removal of the which-path information for the two decay probabilities is necessary to reveal polarisation entanglement. We can list three approaches to this problem two of which have shown success.

The first method is to be oblivious! That is, let us focus only on the subset of emission events that cannot reveal the path information. The finite spectral width of excitons still allows a region of spectral overlap (and thus indistinguishability) where spectral pre-selection of excitons in this overlap region, roughly in the middle of split X^0 energy levels, will remove the information on decay paths albeit the heavy cost of detection rates. Akopian and co-workers have done just that to show correlations that reach beyond the classical bounds for the two photons generated by such a biexciton–exciton decay from a single quantum dot [37].

The second method approached the problem from the materials side: the excitonic exchange splitting to a certain extent originates from the shape anisotropy of the quantum dots. Therefore, physically altering the shape of the quantum dots after growth process has been completed will also alter this undesired level splitting. Stevenson et al. used post-growth annealing of the QD sample which led to a systematic reduction of the exchange splitting as a function of annealing time, as can be seen in Figure 14(*a*) for two different QDs [38,39]. Since every QD starts from a different splitting value within a statistical distribution, a certain annealing range provides a subset of QDs where exchange splitting is effectively removed, and thus results in polarisation correlations that reach beyond the classical bounds without sub-selecting the emission spectrum. To verify entanglement in the emitted photon pairs, Figure 14(*b*) presents full state tomography of the emitted photons in the linear polarisation basis. The inset of the figure is the results of various entanglement tests performed on the measured density matrix [40].

The final method we mention was in fact the first one proposed, but is still yet to be realised: coupling an optical transition to a cavity mode *coherently* broadens the spectrum of the emitted photons due to a reduction of the radiative lifetime, known as the Purcell effect. We will not discuss emitter–cavity coupling in this article; however, it suffices to note that the path distinguishability can be removed by increasing the spectral overlap of the two excitonic transitions via cavity-induced broadening [41]. This method not only recovers polarisation-only entanglement, but further increases the photon-pair generation rate – both features desirable for QIS applications.

4.3. *A quantum gate with excitonic qubits*

Another application we would like to highlight is the possibility to use the QD exciton as the physical representation of a qubit. In 2003, the two-colour version of the pump–probe transient nonlinear spectroscopy technique was utilised along with the linear polarisation selection rules of a quantum dot exciton and biexciton transitions in order to operate a quantum gate. We saw in the previous section that the cascaded decay process of a biexciton follows either of the two decay paths into the ground state. Here, Gammon et al. approached from the other direction where a large value for S is favoured and demonstrated the conditionality of the biexciton generation on the initial exciton polarisation [42]. The excitonic states of Figure 15(*a*) can be interpreted via two-qubit logic states. A laser pulse resonant with the

exciton–biexciton transition was labelled as the 'operation' and had an effect on the quantum dot excitation that is conditional on the initial condition. For example, if the quantum dot was in the $|00\rangle$ or $|01\rangle$ state, the operation left the system unaltered due to either frequency or polarisation selectivity. If, however, the initial state was $|10\rangle$ the 'operation' pulse resulted in a π -excitation to the biexciton state $e^{i\pi}|11\rangle$, while the initial state of $|11\rangle$ dropped to $|10\rangle$ through stimulated emission. Consequently, one could construct a truth table for this effective two-qubit operation that is analogous to a controlled rotation (CROT) gate. Verification of this operation and quantifying the gate's fidelity still relied directly on the transient pump–probe technique discussed earlier. In Figure 15(*b*) the reconstructed physical truth table for this excitonic gate is presented. The system is prepared in the various input states, the operational pulse is applied, and the final state ofthe QD is determined. Ideal operation corresponds to the four white bars having a value of 1 and the rest 0.

4.4. *Initialisation and coherent rotation of quantum dot spin qubits*

All nonresonant excitation mechanisms introduce multiple carriers into the quantum dot levels, whereas resonant excitations only create single excitons within

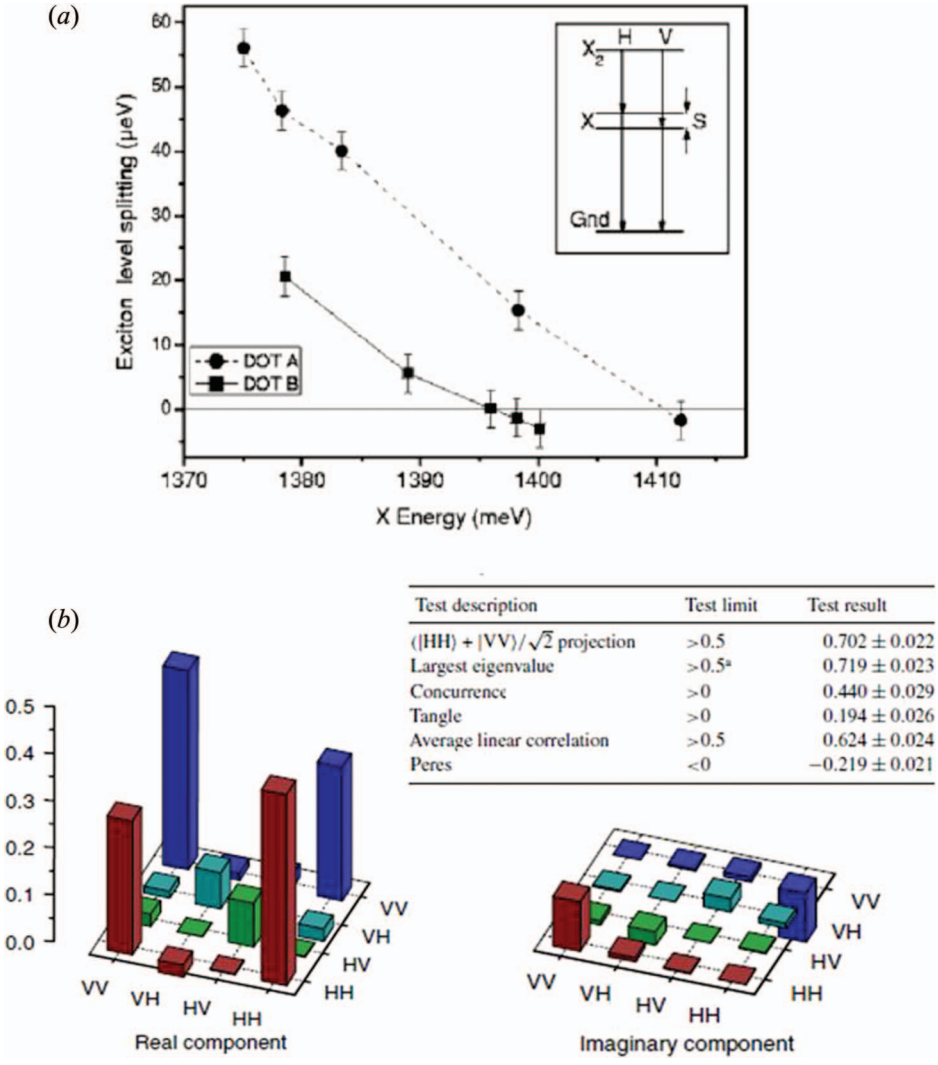

Test description	Test limit	Test result
$(\|HH\rangle + \|VV\rangle)/\sqrt{2}$ projection	>0.5	0.702 ± 0.022
Largest eigenvalue	>0.5[a]	0.719 ± 0.023
Concurrence	>0	0.440 ± 0.029
Tangle	>0	0.194 ± 0.026
Average linear correlation	>0.5	0.624 ± 0.024
Peres	<0	-0.219 ± 0.021

Figure 14. (*a*) In the inset, *S* depicts the fine structure splitting of the neutral exciton X^0 (see Figure 3(*a*)) as a result of the electron–hole exchange interaction. The data points represent how the fine structure splitting can be tuned through annealing two different InAs QD samples for 5 min intervals at 675°C. For generating polarisation entangled photons from QD emission the third data point for DOT B is of interest [39]. (*b*) The real and imaginary components of the measured density matrix for the two-photon state emitted from a QD with an exchange splitting less than 1.3 μeV. Inset: The results of various entanglement tests performed on the measured density matrix [40].

the quantum dot. The unprecedented spectral resolution provided by the differential transmission techniques highlighted above allow direct access to the transitions between the individual fine structure and Zeeman levels. We showed in Figure 12 how this accessibility can be used for spectroscopic measurements to reveal the strength of electron–hole exchange interaction and quantum dot anisotropy. In the case of a single excess electron trapped in a quantum dot, we do not have *a priori* control, over or

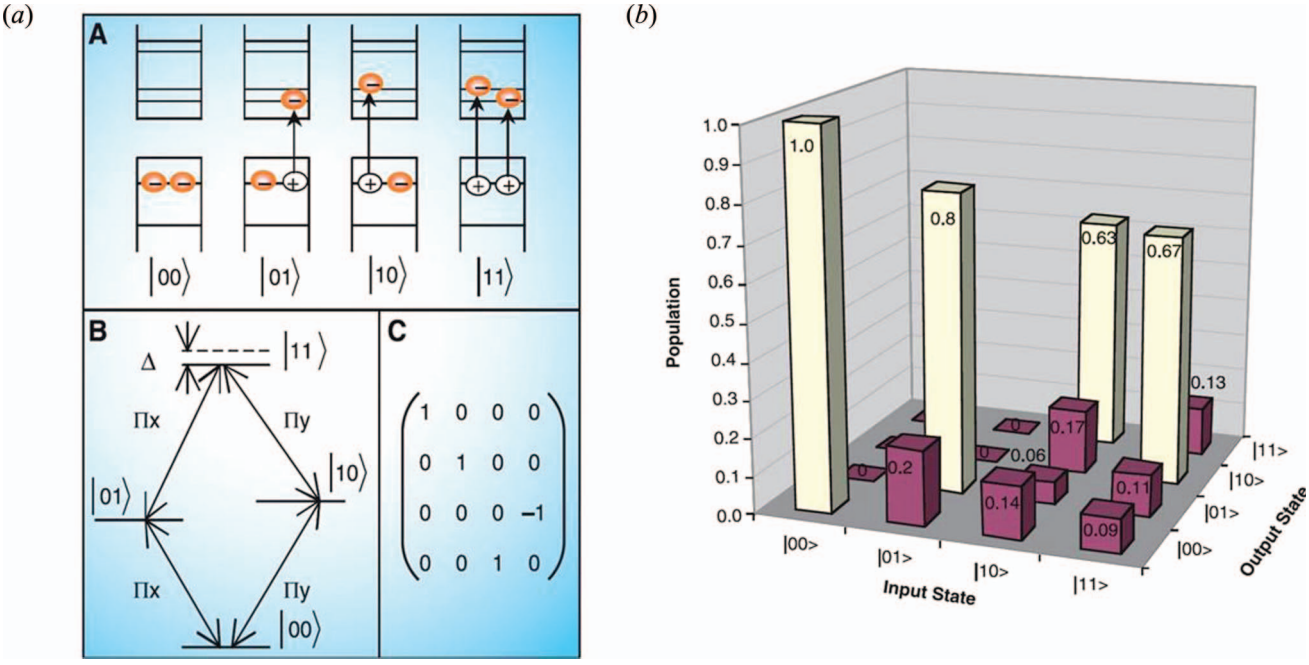

Figure 15. Controlled Rotation (CROT) gate based on QD biexciton and exciton transitions. (*a*) Panel A is a schematic of the QD states relevant to the CROT gate. Panel B is the excitation energy level diagram and Panel C is the CROT gate transformation matrix (note $|10\rangle$ is transformed to $-|11\rangle$). (*b*) The reconstructed physical truth table for the CROT gate. The operational pulse is a π -pulse tuned to the $|10\rangle - |11\rangle$. The system is prepared in the various input states, the operational pulsed is applied, and the final state of the QD is determined. Ideal operation corresponds to the four white bars having a value of 1 and the rest 0 [42].

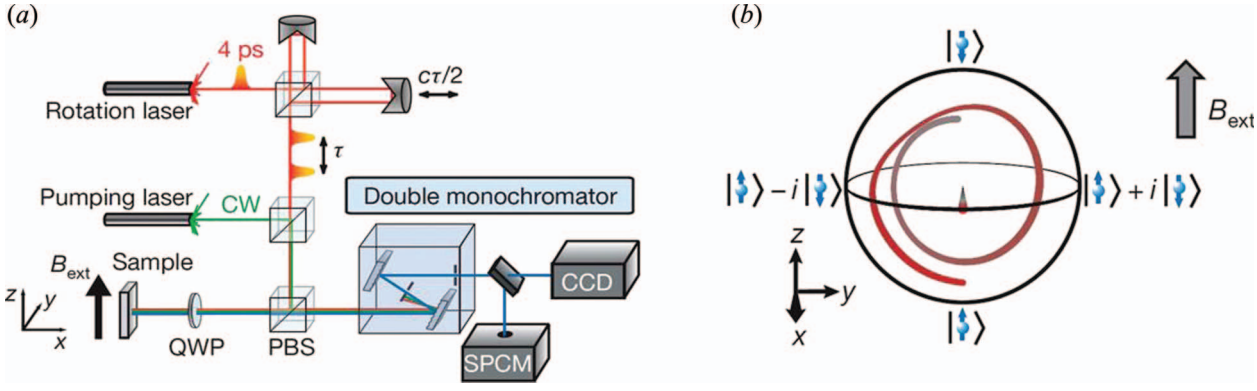

Figure 16. (*a*) Experimental setup for pulsed optical rotation of QD spin. During each experimental cycle, one or two rotation pulses may be sent to the sample to observe Rabi oscillations or Ramsey interference, respectively. The time delay, τ, between pairs of pulses is controlled by a retroreflector mounted on a computer-controlled translation stage. CW, continuous wave; QWP, quarter-wave plate; PBS, polarising beam splitter; SPCM, single-photon counting module; CCD, charge-coupled device; c, speed of light. (*b*) Reconstructed evolution of the Bloch vector. The curves trace out the tip of the Bloch vector in the one-pulse (Rabi oscillation) experiment. The colour scale indicates the length of the Bloch vector, which shrinks exponentially as the system is evolved for longer times. Views are from the perspective of the x axis [44].

knowledge of, its spin. In atomic physics, the concept of optical pumping is used to create an imbalance in the spin projection of the ground states of an atomic ensemble. This process relies on the fact that upon excitation to a higher electronic state, the atoms will decay randomly into a set of ground states in accordance with the strength of the corresponding transition matrix elements. In charged quantum dots, such as the trion in Figure 3, the process can not work in ideal conditions, but in the presence of state mixing mechanisms such as nuclear spin coupling and hole mixing, there is small but finite rate of decay into the other electron ground state. Specifically, if a resonant laser drives the σ^+ transition, there is a small, but finite probability for a spontaneous Raman spin flip process to take place and shelve the electron in the spin down ground state. The system then goes dark and no more light is scattered due to both frequency and polarisation selection rules. This exact idea, an outgrowth of the previously discussed DT technique, has been demonstrated in [43], where a QD electron was optically pumped and thus prepared a given spin state with 99.8% fidelity. This is the initial step of any QIP protocol utilising single QD spins.

Finally, we briefly touch on a recent work that demonstrates coherent control of individual electron spin states using ultrafast optical pulses and optically induced spin rotations. The spin of a singly charged QD serves as the qubit. The sample is placed in a static magnetic field perpendicular to the growth direction (the Voigt geometry). If a single electron is loaded into the QD, it will coherently precess around the applied perpendicular field at the Larmor frequency. Visualised on the Bloch sphere the state of the electron spin is traversing a great circle of the sphere ignoring any spin dephasing effects. Application of a circularly polarised ultrafast optical pulse red-detuned from the electron transition Stark shifts the two ground state electronic levels and results in spin precession around the direction parallel to the QD growth direction (perpendicular to the externally applied magnetic field). The key point is that the optical pulse, via the dynamic Stark effect, acts as an ultrafast effective magnetic field and induces coherent spin rotation. Figure 16(*a*) is the experimental setup employed to optically evolve the electron spin and Figure 16(*b*) is the reconstructed evolution of the Bloch vector. We direct the reader to [44,45] for a more detailed discussion of the two approaches, but the main message here is that coherent optical rotation of a single QD spin has now been observed 10 years after the first photon correlation measurements indicating nonclassical light emission from QDs.

5. Conclusion

Given that the word *spectroscopy* comprises two roots (one Latin and one Greek) meaning appearance-watching, one may be led to believe that spectroscopy indeed goes all the way back to the Greeks and Romans. Surprisingly, this powerful word itself was not coined until 1882 by Arthur Schuster in order to classify studies focused on the spectral properties of light–matter interaction. With this particular definition, the first systematic spectroscopy experiments were performed two centuries earlier. In 1666 Sir Isaac Newton demonstrated the multi-colour nature of sunlight by using a glass prism which was readily available from the local market as a 'Fool's Paradise'. His simple but ground-breaking findings initiated 350 years of investigations performed on light absorbed, scattered, and emitted by matter. Today, spectroscopy has generated a sea of knowledge on the nature of light and its interaction with matter, where QD research constitutes a modest component. We tried to give a brief survey of the optical measurement techniques utilised to investigate the physics of quantum dots. Today, thanks to these studies we now have a high-level of control over the physics of QDs and we can expect to see a continuation of productivity in quantum dot research in the coming years with less emphasis on observation and more on control. The optical techniques used for this progress, however, will likely be a combination of what we discussed here, as the general principles of spectroscopy are here to stay.

Notes on contributors

Nick Vamivakas is a postdoctoral fellow in the Cavendish Laboratory at the University of Cambridge since 2007 supported by QIP IRC (GR/S82176/01) and EPSRC Grant no. EP/G000883/1. He received his Bachelor of Science degree in 2001 from Boston University ECE Department and received his Ph.D. from the OCN Laboratory at Boston University in 2007 under the supervision of Professors Swan, Unlu and Goldberg.

Mete Atatüre is a Lecturer in the Cavendish Laboratory at the University of Cambridge. He received his Bachelor of Science degree in 1996 from Bilkent University Physics Department in Turkey. Then, he joined the Quantum Imaging Laboratory at Boston University for his Ph.D. studies until 2002. From 2002 to 2007, he worked as a Postdoctoral Fellow in the Quantum Photonics Group at ETH Zurich. Current research efforts of his research group include

optical control of single and multiple quantum-dot spins, high-resolution spectroscopy of diamond-based emitters, and nanoplasmonics.

Suggested reading

(i) H. Haug and S.W. Koch, *Quantum Theory of the Optical and Electronic Properties of Semiconductors*, 3rd ed., World Scientific, Singapore, 2001, pp. 44–48.

(ii) R. Loudon, *The Quantum Theory of Light*, 3rd ed., Oxford University Press, Oxford, 2004.

(iii) V.V. Mitrin, V.A. Kochelap, and M.A. Stroscio, *Quantum Heterostructures: Microelectronics and Optoelectronics*, Cambridge University Press, Cambridge, 1999.

(iv) S. Mukamel, *Principles of Nonlinear Optical Spectroscopy*, Oxford University Press, New York, 1995.

(v) U. Woggon, *Optical Properties of Semiconductor Quantum Dots*, Springer, Berlin, 1996.

(vi) L. Jacak, P. Hawrylak, and A. Wojs, *Quantum Dots*, Springer, Berlin, 1998.

(vii) D. Bimberg, M. Grundmann, N.N. Ledentsov, *Quantum Dot Heterostructures*, Wiley, Chichester, UK, 1999.

(viii) D.D. Awschalom, D. Loss, and N. Samarth, *Semiconductor Spintronics and Quantum Computation*, Springer, Berlin, 2002.

(ix) P.M. Petroff, A. Lorke, and A. Imamoglu, *Epitaxially self-assembled quantum dots*, Phys. Today 54 (2001), pp. 46–52.

(x) D. Gammon and D.G. Steel, *Optical studies of single quantum dots*, Phys. Today 55 (2002), pp. 36–41.

(xi) M. Bayer, G. Ortner, O. Stern, A. Kuther, A.A. Gorbunov, A. Forchel, P. Hawrylak, S. Fafard, K. Hinzer, T.L. Reinecke, S.N. Walck, J.P. Reithmaier, F. Klopf, and F. Schäfer, *Fine structure of neutral and charged excitons in self-assembled In(Ga)As/(Al)GaAs quantum dots*, Phys. Rev. B 65 (2002), 195315:1–23.

References

[1] E.F. Schubert, *Delta-doping of Semiconductors*, Cambridge University Press, Cambridge, 1996.

[2] J.H. Blokland, M. Bozkurt, J. M. Ulloa, D. Reuter, A.D. Wieck, P.M. Koenraad, P.C.M. Christianen, and J.C. Maan, *Ellipsoidal InAs quantum dots observed by cross-sectional scanning tunneling microscopy*, Appl. Phys. Lett. 94 (2009), 023107:1–3.

[3] H. Haug and S.W. Koch, *Quantum Theory of the Optical and Electronic Properties of Semiconductors*, 3rd ed., World Scientific, Singapore, 2001, pp. 44–48.

[4] G. Bester, S. Nair, and A. Zunger, *Pseudopotential calculation of the excitonic fine structure of million-atom self-assembled In_{1-x} Ga_xAs/GaAs quantum dots*, Phys. Rev. B 67 (2003), 161306:1–4.

[5] A. Zunger, *Pseudopotential theory of semiconductor quantum dots*, Phys. Stat. Sol. (b) 224 (2001), pp. 727–734.

[6] M. Bayer, G. Ortner, O. Stern, A. Kuther, A.A. Gorbunov, A. Forchel, P. Hawrylak, S. Fafard, K. Hinzer, T.L. Reinecke, S.N. Walck, J.P. Reithmaier, F. Klopf, and F. Schäfer, *Fine structure of neutral and charged excitons in self-assembled In(Ga)As/(Al)GaAs quantum dots*, Phys. Rev. B 65 (2002), 195315:1–23.

[7] R.J. Warburton, B.T. Miller, C.S. Durr, C. Bodefeld, K. Karrai, J.P. Kotthaus, G. Medeiros-Ribeiro, P.M. Petroff, and S. Huant, *Coulomb interactions in small charge-tunable quantum dots: a simple model*, Phys. Rev. B 58 (1998), pp. 16221–16231.

[8] J.-Y. Marzin, J.-M. Gérard, A. Izraël, D. Barrier, and G. Bastard, *Photoluminescence of single InAs quantum dots obtained by self-organized growth on GaAs*, Phys. Rev. Lett. 73 (1994), pp. 716–719.

[9] D. Leonard, M. Krishnamurthy, C.M. Reaves, S.P. Denbaars, and P.M. Petroff, *Direct formation of quantum-sized dots from coherent islands of InGaAs on GaAs surfaces*, Appl. Phys. Lett. 63 (1993), pp. 3203–3205.

[10] E. Dekel, D.V. Regelman, D. Gershoni, E. Ehrenfreund, W.V. Schoenfeld, and P.M. Petroff, *Radiative lifetimes of single excitons in semiconductor quantum dots – manifestation of the spatial coherence effect*, Sol. St. Comm. 117 (2001), pp. 395–400.

[11] U. Woggon, *Optical Properties of Semiconductor Quantum Dots*, Springer, Berlin, 1996.

[12] C. Santori, D. Fattal, J. Vuèkoviæ, G.S. Solomon, E. Waks, and Y. Yamamoto, *Submicrosecond correlations in photoluminescence from InAs quantum dots*, Phys. Rev. B 69 (2004), 205324:1–8.

[13] J.M. Smith, P.A. Dalgarno, R.J. Warburton, A.O. Govorov, K. Karrai, B.D. Gerardot, and P.M. Petroff, *Voltage control of the spin dynamics of an exciton in a semiconductor quantum dot*, Phys. Rev. Lett. 94 (2005), 197402:1–4.

[14] V. Zwiller, T. Aichele, and O. Benson, *Single-photon Fourier spectroscopy of excitons and biexcitons in single quantum dots*, Phys. Rev. B 69 (2004), 165307:1–4.

[15] C. Becher, A. Kiraz, P. Michler, A. Imamoğlu, W.V. Schoenfeld, P.M. Petroff, L. Zhang, and E. Hu, *Nonclassical radiation from a single self-assembled InAs quantum dot*, Phys. Rev. B 63 (2001), 121312(R).

[16] R. Loudon, *The Quantum Theory of Light*, 3rd ed., Oxford University Press, Oxford, 2004.

[17] P. Kumar, P. Kwiat, A. Migdall, S.W. Nam, J. Vuckovic, and F.N.C. Wong, *Photonic technologies for quantum information processing*, Quant. Inf. Proc. 3 (2004), pp. 215–231.

[18] W. Slysz, M. Wegrzecki, J. Bar, P. Grabiec, M. Gorska, V. Zwiller, C. Latta, P. Bohi, I. Milostnaya, O. Minaeva, A. Antipov, O. Okunev, A. Korneev, K. Smirnov, B. Voronov, N. Kaurova, G. Gol'tsman, A. Pearlman, A. Cross, I. Komissarov, and R. Sobolewski, *Fiber-coupled single photon detectors based on NbN superconducting nanostructures for practical quantum cryptography and photon-correlation studies*, Appl. Phys. Lett. 88 (2006), 261113:1–3.

[19] A. Kiraz, S. Fälth, C. Becher, B. Gayral, W.V. Schoenfeld, P.M. Petroff, L. Zhang, E. Hu, and A. Imamoğlu, *Photon correlation spectroscopy of a single quantum dot*, Phys. Rev. B 65 (2002), 161303(R).

[20] A. Kiraz, M. Atatüre, and A. Imamoğlu, *Quantum-dot single-photon sources: prospects for applications in linear optics quantum-information processing*, Phys. Rev. A 69 (2004), 032305.

[21] S. Mukamel, *Principles of Nonlinear Optical Spectroscopy*, Oxford University Press, New York, 1995.

[22] T.H. Stievater, X. Li, D.G. Steel, D. Gammon, D.S. Katzer, and D. Park, *Transient nonlinear spectroscopy of excitons and biexcitons in single quantum dots*, Phys. Rev. B 65 (2002), 205319.

[23] W. Langbein, P. Borri, U. Woggon, V. Stavarache, D. Reuter, and A.D. Wieck, *Radiatively limited dephasing in InAs quantum dots*, Phys. Rev. B 70 (2004), 033301.
[24] P. Borri and W. Langbein, *Four-wave mixing dynamics of excitons in InGaAs self-assembled quantum dots*, J. Phys.: Cond. Mat. 19 (2007), 295201.
[25] P. Borri, W. Langbein, S. Schneider, U. Woggon, R.L. Sellin, D. Ouyang, and D. Bimberg, *Ultralong dephasing time in InGaAs quantum dots*, Phys. Rev. Lett. 87 (2001), 157401.
[26] B. Alén, F. Bickel, K. Karrai, R.J. Warburton, and P.M. Petroff, *Stark-shift modulation absorption spectroscopy of single quantum dots*, Appl. Phys. Lett. 83 (2003), ppp. 2235–2237.
[27] A. Högele, S. Seidl, M. Kroner, K. Karrai, R.J. Warburton, B.D. Geradot, and P.M. Petroff, *Voltage-controlled optics of a quantum dot*, Phys. Rev. Lett. 93 (2004), 217401.
[28] M. Kroner, A. Högele, S. Seidl, R.J. Warburton, B.D. Gerardot, A. Badolato, P.M. Petroff, and K. Karrai, *Voltage-controlled linewidth of excitonic transitions in a single self-assembled quantum dot*, Phys. E 32 (2006), ppp. 61–64.
[29] B. Alén, A. Högele, M. Kroner, S. Seidl, K. Karrai, R.J. Warburton, A. Badolato, G. Medeiros-Ribeiro, and P.M. Petroff, *Absorptive and dispersive optical responses of excitons in a single quantum dot*, Appl. Phys. Lett. 89 (2006), 123124.
[30] S.M. Mansfield and G.S. Kino, *Solid immersion microscope*, Appl. Phys. Lett. 57 (1990), ppp. 2615–2616.
[31] B.D. Gerardot, S. Seidl, P.A. Dalgarno, R.J. Warburton, M. Kroner, K. Karrai, A. Badolato, and P.M. Petroff, *Contrast in transmission spectroscopy of a single quantum dot*, Appl. Phys. Lett. 90 (2007), 221106.
[32] A.N. Vamivakas, M. Atatüre, J. Dreiser, S.T. Yilmaz, A. Badolato, A.K. Swan, B.B. Goldberg, A. Imamoğlu, and M.S. Ünlü, *Strong extinction of a far-field laser beam by a single quantum dot*, Nano Lett. 7 (2007), pp. 2892–2896.
[33] P. Michler, A. Kiraz, C. Becher, W.V. Schoenfeld, P.M. Petroff, L. Zhang, E. Hu, and A. Imamoğlu, *A quantum dot single-photon turnstile device*, Science 290 (2000), pp. 2282–2285.
[34] E. Waks, K. Inoue, C. Santori, D. Fattal, J. Vuckovic, G.S. Solomon, and Y. Yamamoto, *Quantum cryptography with a photon turnstile*, Nature 420 (2002), p. 762.
[35] C. Santori, D. Fattal, J. Vuckovic, G.S. Solomon, and Y. Yamamoto, *Indistinguishable photons from a single-photon device*, Nature 419 (2002), p. 594.
[36] A. Aspect, P. Grangier, and G. Roger, *Experimental tests of realistic local theories via Bell's theorem*, Phys. Rev. Lett. 47 (1981), ppp. 460–463.
[37] N. Akopian, N.H. Lindner, E. Poem, Y. Berlatzky, J. Avron, D. Gershoni, B.D. Gerardot, and P.M. Petroff, *Entangled photon pairs from semiconductor quantum dots*, Phys. Rev. Lett. 96 (2006), 130501.
[38] R.M. Stevenson, R.J. Young, P. Atkinson, K. Cooper, D.A. Ritchie, and A.J. Shields, *A semiconductor source of triggered entangled photon pairs*, Nature 439 (2006), pp. 179–182.
[39] D.J.P. Ellis, R.M. Stevenson, R.J. Young, A.J. Shields, P. Atkinson, and D.A. Ritchie, *Control of fine-structure splitting of individual InAs quantum dots by rapid thermal annealing*, Appl. Phys. Lett. 90 (2007), 011907.
[40] R.J. Young, R.M. Stevenson, P. Atkinson, K. Cooper, D.A. Ritchie, and A.J. Shields, *Improved fidelity of triggered entangled photons from a single quantum dots*, New J. Phys. 8 (2006), 29:1–9.
[41] T.M. Stace, G.J. Milburn, and C.H.W. Barnes, *Entangled two-photon source using biexciton emission of an asymmetric quantum dot in a cavity*, Phys. Rev. B 67 (2003), 085317:1–15.
[42] X. Li, Y. Wu, D. Steel, D. Gammon, T.H. Stievater, D.S. Katzer, D. Park, C. Piermarocchi, and L.J. Sham, *An all-optical quantum gate in a semiconductor quantum dot*, Science 301 (2003), pp. 809–811.
[43] M. Atatüre, J. Dreiser, A. Badolato, A. Högele, K. Karrai, and A. Imamoğlu, *Quantum-dot spin-state preparation with near-unity fidelity*, Science 312 (2006), pp. 551–553.
[44] D. Press, T.D. Ladd, B. Zhang, and Y. Yamamoto, *Complete quantum control of a single quantum dot spin using ultrafast optical pulses*, Nature 456 (2008), pp. 218–221.
[45] J. Berezovsky, M.H. Mikkelsen, N.G. Stoltz, L.A. Coldren, and D.D. Awschalom, *Picosecond coherent optical manipulation of a single electron spin in a quantum dot*, Science 320 (2008), pp. 349–352.